


Article

Study on Wear and Scour Performance of Ni6035WC/Wc-10Cr-4Cr Coating by HVOF

Xinghua Liang^{1,†}, Tong Zhuang^{1,†}, Lingxiao Lan^{1,†}, Jian Huang², Siying Li^{1,*} , Yunsheng Lei³, Bohan Xu², Yujiang Wang¹, Xueli Shi¹ and Qicheng Hu^{1,*}

¹ Guangxi Key Laboratory of Automobile Components and Vehicle Technology, Guangxi University of Science & Technology, Liuzhou 545006, China; 100001090@gxust.edu.cn (X.L.); 17861136880@163.com (T.Z.); llx2685062@163.com (L.L.); 13152528815@163.com (Y.W.); s1659186234@163.com (X.S.)

² Foshan Taoyuan Advanced Manufacturing Research Institute, Foshan 528225, China; huangjian@gdinm.com (J.H.); xubohan19950917@163.com (B.X.)

³ Guangdong Yueke New Material Technology Co., Ltd., Foshan 528225, China; aliu620@163.com

* Correspondence: lisiying@gxust.edu.cn (S.L.); huqicheng@gmail.com (Q.H.)

† These authors contributed equally to this work.

Abstract: The Ni6035WC/WC-10Co-4Cr wear- and scour-resistant composite coating was fabricated using supersonic flame spraying technology. To further enhance the wear and scour resistance of the HVOF-sprayed Ni6035WC/WC-10Co-4Cr composite coatings, a post-treatment was conducted via vacuum remelting. This involved placing the coatings in a vacuum sintering process at 1120 °C for 10 min. Scanning electron microscopy (SEM), X-ray diffraction (XRD), and hardness testing were employed to characterize the structure and morphology of the Ni6035WC/WC-10Co-4Cr coating, as well as to assess its wear and scour resistance. The results indicate that vacuum sintering significantly enhances the wear and scour resistance of the coating, while also improving its hardness, density, and bonding strength. The hardness of each coating after vacuum sintering, 1019 HV, 920 HV, and 897 HV, was improved by 6% compared to 966 HV, 906 HV, and 845 HV before sintering. The average wear rate of each coating after sintering was 13% lower than before vacuum sintering. Furthermore, the impact of varying WC-10Co-4Cr content on the coating's properties was examined under identical test conditions. It was found that the optimal overall performance was achieved with a WC-10Co-4Cr content of 20%, resulting in an average wear rate that was 19% lower than that of other coatings.

Keywords: HVOF; vacuum sintering; abrasion resistance; scour resistance



Citation: Liang, X.; Zhuang, T.; Lan, L.; Huang, J.; Li, S.; Lei, Y.; Xu, B.; Wang, Y.; Shi, X.; Hu, Q. Study on Wear and Scour Performance of Ni6035WC/Wc-10Cr-4Cr Coating by HVOF. *Coatings* **2024**, *14*, 1148. <https://doi.org/10.3390/coatings14091148>

Academic Editor: Vincent Ji

Received: 3 August 2024

Revised: 2 September 2024

Accepted: 5 September 2024

Published: 6 September 2024



Copyright: © 2024 by the authors. Licensee MDPI, Basel, Switzerland. This article is an open access article distributed under the terms and conditions of the Creative Commons Attribution (CC BY) license (<https://creativecommons.org/licenses/by/4.0/>).

1. Introduction

HVOF is a novel deposition technology developed in recent years [1,2]; the HVOF spraying method typically generates higher particle velocities, leading to higher kinetic energy and, due to the lower flame temperature, the particle temperatures are also lower compared to other spraying techniques like high-velocity oxy-fuel (HVOF) [3–5]. With the latest generation of torches, HVOF has become an alternative to other spraying for commercial use [1,6]. High particle velocities are often favored due to its positive effect on coating denseness and cohesion, whereas high particle temperatures are generally avoided due to increased decarburization and the formation of brittle structures in the coating [7,8], such that the deposited coatings by HVOF can keep the excellent wear resistance of the ceramic. The coating material is heated to a molten or semi-molten state by the combustion-supporting gas in the combustion chamber. Then, it is rapidly cooled and solidified on the metal substrate with a high-speed jet flame flow to form a dense coating. The mechanical bonding between the coating and the substrate does not damage the substrate, which is convenient for coating repair and refurbishments [9]. (Therefore, no oxidation atmosphere exists in the spraying environment, and the oxidation of the sprayed powders are avoided as far as possible.) In HVOF spraying, the absence of an oxidizing atmosphere minimizes the

oxidation of the sprayed powder. These advantages are particularly suitable for spraying WC-based powder [10]. A potential disadvantage of using HVOF or HVOF to deposit hard coatings is the inherent defects that include porosity, oxidation and decomposition of particles, and residual stresses, etc., [11–13]. These microstructural defects within the coating can weaken cohesion and adhesion, lead to fracture and spalling, and adversely affect wear resistance [14].

Due to the chemical inhomogeneity in the coating during the spraying process, the coating does not metallurgically bond with the substrate. However, vacuum sintering technology, a modern surface metallurgy technique, can effectively alter the microstructure, composition, and properties of the substrate's working surface [15]. Heat treatment conducted in a vacuum or controlled atmosphere can minimize decarburization, thereby enhancing the wear resistance of WC-based coatings [16].

Mishra et al. [17] studied the effects of heat treatment on WC-12Co coatings at various temperatures, demonstrating that heat treatment significantly improves both mechanical properties and microstructural characteristics. Similarly, Chen et al. [18] investigated the effect of post-heat treatment (PHT) on laser-deposited $WxC + Ni$ -based composite thin walls and found that heat treatment enhances the coating quality. Furthermore, M. Giacomantonio et al. [19] discovered that heat treatment can successfully eliminate defects, provide a more uniform microstructure, and improve the microhardness, adhesive strength, and tribological properties of composite coatings. Matikainen et al. [20] sprayed two coatings, Cr3C2-50NiCrMoNb and Cr3C2-37WC-18NiCoCr, using WC-10Co4Cr as a reference material. The results showed that Cr3C2-37WC-18NiCoCr improved both the abrasion resistance and the resistance of the coating to the erosion of dry particles. Torkashvand et al. [21] evaluated the wear performance of HVOF-sprayed WC-based composite coatings with co-lean or co-free binders as alternatives to conventional WC-CoCr wear-resistant layers. The coatings exhibited good high-temperature friction and wear properties. Zhang et al. [14] investigated the effect of different heat treatment temperatures on the hardness and wear resistance of HVOF-sprayed WC-Cr3C2-Ni coatings. They derived a wear equation, $W = 6 \times 10^{-7} \times \mu/H$, describing the relationship between the wear rate, coefficient of friction, and hardness of the WC-Cr3C2-Ni coatings heat-treated at 550–1000 °C.

Mishra, T. K. et al. [22] prepared Ni-10WC coatings using HVOF (high-velocity oxy-fuel) and subsequently heat-treated the coatings in an electric muffle furnace at various temperatures for 30 min to enhance wear resistance. The study found that the coatings exhibited optimal wear resistance at 600 °C, although the hardness and porosity were only average. This outcome is attributed to the following two factors: first, the Ni-10WC coatings prepared by HVOF are prone to decarburization; second, the coatings are susceptible to high-temperature oxidation during heat treatment without atmospheric protection. Zhang et al. [23] demonstrated that the WC-Cr3C2-Ni coatings applied to copper substrates significantly improved the substrates' wear resistance. However, the porosity of these coatings was twice as high as that of the coatings in the present study, which could negatively impact the coatings' stability and service life. Tian et al. [24] attempted to enhance the performance of the HVOF-sprayed WC-10Co4Cr coatings by post-sealing them with epoxy resin using vacuum impregnation. While this surface sealing method improved the external surface, it failed to enhance the internal bonding of the coatings. Consequently, the bonding strength of the WC-10Co4Cr metal–ceramic coatings was generally weaker compared to the composite coatings in this study, leading to reduced resistance to erosion.

In this work, we focused on the changes in the comprehensive properties of the coatings, such as wear resistance and scour resistance, following vacuum remelting at 1120 °C. It was found that the coatings produced by vacuum remelting exhibited superior properties compared to those obtained through vacuum heat treatment at lower temperatures [19,25,26]. Additionally, the effects of incorporating different ratios of WC-10Co-4Cr on the overall performance of the coatings were investigated. The microstructure of the

coatings was analyzed, Vickers hardness was measured, and the tribological behavior was evaluated under rotational frictional wear at room temperature.

2. Materials and Methods

2.1. Materials

The substrate material used in this experiment is 316 stainless steel, and the specimen specifications are $\Phi 40 \times 8$ mm friction wear samples, $\Phi 25$ mm long 330 mm round bar samples, and $40 \times 80 \times 3$ mm metallographic samples, respectively. The spraying materials are Ni6035WC, WC-10Co-4Cr and Ni35A powders prepared by Chengdu Daguang, Chengdu, China, with particle sizes of $140/325 \mu\text{m}$, $5/30 \mu\text{m}$, and $150/300 \mu\text{m}$, respectively, and the main chemical compositions of the materials are shown in Table 1.

Table 1. Chemical composition of Ni35A, Ni6035WC, and WC-10Co-4C powder.

Type	Element (wt.%)	C	B	Si	Cr	Fe	Cu	Ni	W	Co	O
Ni35A	Content	0.23	1.26	2.56	7.25	5.05	14.58	Bal.	-	-	-
Ni6035WC	Content	1.49	2.01	2.74	12.55	4.86	-	Bal.	34.36	-	-
WC-10Co-4Cr	Content	5.46	-	-	3.88	0.27	-	-	Bal.	10.28	0.15

2.2. Coating Fabrication

To investigate the effect of varying WC-10Co-4Cr content on the structure and properties of the coating, the following three different compositions were tested: 20% WC-10Co-4Cr, 30% WC-10Co-4Cr, and 40% WC-10Co-4Cr. The compositions of the different WC-10Co-4Cr/Ni6035WC composite powders are detailed in Table 2. As shown in Figure 1, the powder particles exhibit a spherical morphology. This spherical shape significantly enhances the fluidity of the coating and reduces resistance during the deposition process.

Table 2. Composition of different WC-10Co-4Cr/Ni6035WC composite powders.

Specimen Number	WC-10Co-4Cr	Ni6035WC
1#	40%	60%
2#	30%	70%
3#	20%	80%

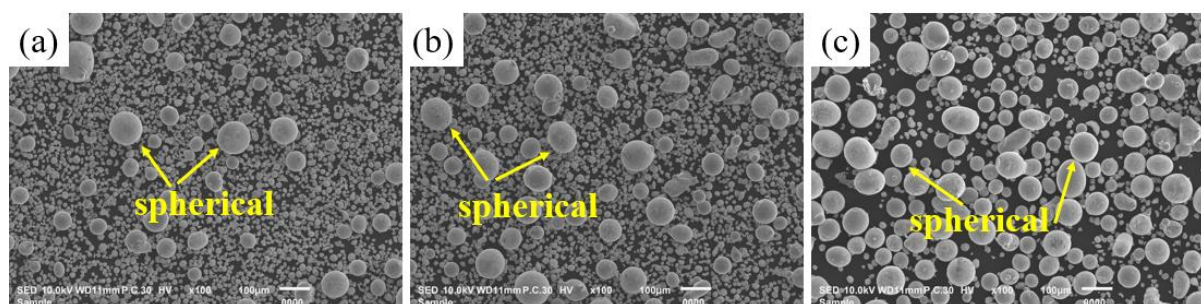


Figure 1. (a) 40%WC-10Co-4Cr + 60% Ni6035WC mixed powder particle size morphology; (b) 30%WC-10Co-4Cr + 70% Ni6035WC mixed powder particle size morphology; (c) 20%WC-10Co-4Cr + 80% Ni6035WC mixed powder particle size morphology.

The coating preparation followed the procedures described in references [27–29]. The mixed powder, combined with a set of stirred steel balls (each with a diameter of 15 mm), was placed in a sealed iron drum and mixed using a drum mixer for 1.5 h. Subsequently, the powder was baked at 70°C for 1.5 h. The substrate specimen was roughened by sandblasting and, following the sandblasting, any surface residues were removed using an air gun. The powder was then immediately sprayed onto the substrate within 2 h of

the cleaning process. The prepared substrate was thoroughly cleaned, and any oil or oxide layers on the surface were removed with alcohol.

The spraying process was conducted by a Kermetico/C-01 HVOF (Benicia, CA, USA) system, with the process parameters outlined in Table 3. During the spraying process, an external air duct was employed for cooling, with the air supply being cooled once per spraying cycle according to the established spraying path.

Table 3. The parameters of HVOF spraying.

A						
Coating	Powder Feeding Capacity (g/min)	Air/L·min ^{−1}	H ₂ /L·min ^{−1}	N ₂ /L·min ^{−1}	Spray Distance /mm	Walking Speed (mm/s)
Bonding layer Ni35A	35	84	35	23	175	800
Coating 1#, 2#, 3#	60–65	84	235	23	175	800
B						
Spray Parameter				Unit	Value	
Higher temperatures				°C	120	
Fuel 1 (propane) flow				psi	78	
Fuel 2 (propane) flow				psi	78	
Coating Ni35A thickness				μm	110	
Coating 1#, 2#, 3# thickness				μm	230	

The vacuum sintering coating remelting process was carried out using a vacuum furnace on the round bar samples and friction wear samples after spraying. The samples were heat-treated to 1120 °C at the rate of 5 °C/min in vacuum furnace (GSL-1400X), (Hefei Crystal Material Technology Co., Ltd., Hefei, China), which was connected to a molecular vacuum pump to maintain 10³ Pa. Then, the samples were kept under the vacuum atmosphere at the target temperature for 10 min. Subsequently, the samples were naturally cooled to room temperature in the vacuum furnace, As shown in Figure 2. Finally, the samples were taken out for the analysis of microstructure and properties. Figure 3 shows the placement of the samples during the sintering process.

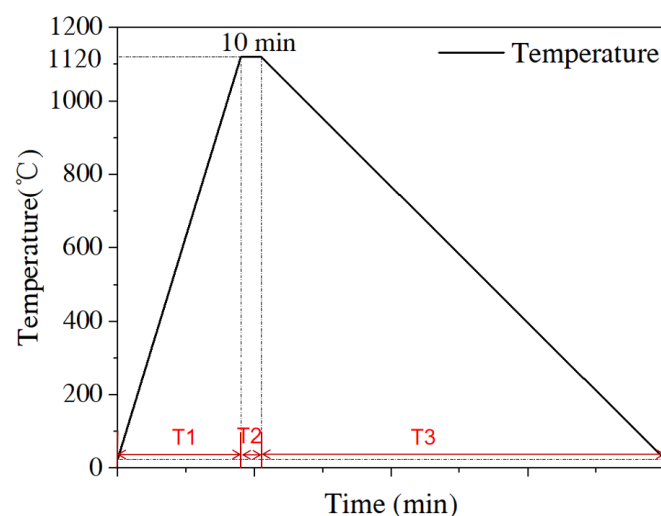


Figure 2. Sintering process curves of three samples in a vacuum furnace. (T1: Heat up to 1120 °C with the highest heating rate of the vacuum furnace; T2: Holding time 10 min; T3: Reduce to room temperature with the furnace, remove the sample).

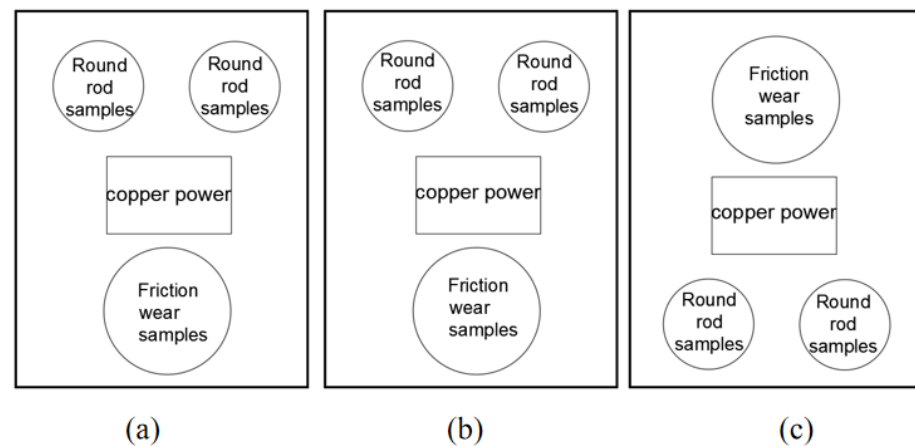


Figure 3. Placement of samples during the sintering process ((a) 1# Powder Coating Sample; (b) 2# Powder Coating Sample; (c) 3# Powder Coating Sample).

2.3. Material Characterization and Performance Testing

First, $5\text{ mm} \times 10\text{ mm} \times 3\text{ mm}$ metallographic samples were cut and polished step by step with metallographic sandpaper, before being mechanically polished to a mirror surface with a polishing solution. After blow-drying, the microstructure was observed with a LEICA DM4M Leica metallographic microscope (Weztlar, Germany). An MH-500D microhardness tester (Shanghai, China) was used for hardness testing of the coating (load 300 g, loading time of 15 s).

The coating was subjected to a friction and wear test according to the G99-05 Standard Test Method for Wear Testing with a Pin-on-Disk Apparatus. Friction and wear experiments were carried out using MS-9000 multifunctional friction tester (Lanzhou, China), and a silicon nitride ball with a radius of 2 mm was selected for the wear vice, with a radius of rotation of 5 mm, a load of 10 N, a test time of 720 min, a rotational speed of 382 rpm, a skidding distance of 8636.3 m.

During the flushing experiment, the sample was assembled onto a small rotary table, rotated at the maximum speed of the small rotary table; the sandblasting nozzle was fixed, the spray distance was set at 100 mm, the angle of sandblasting was set at 90° , the pressure of sandblasting was set at 3 kg, the time of sandblasting was set at 3 min, and the weight loss of the sample before and after sandblasting was recorded. The samples before and after sintering were sliced, and the coated and cut surfaces were flushed, respectively. The spray distance was set at 100 mm, the angle of sandblasting was 90° , the pressure of sandblasting was 3 kg, and the time of sandblasting was 3 min, and the coating shedding of the coated section and the cut surface after flushing were observed.

3. Results and Discussion

3.1. Microstructural Characterization

The microstructures of the cross-sections of the HVOF-sprayed and vacuum-remelted WC-10Co-4Cr/Ni6035WC composite powder coatings are illustrated in Figure 4. Observations of the microstructures in the samples without vacuum remelting reveal several issues. Specifically, the 3# coatings exhibit prominent voids at the coating junctions, along with transverse and longitudinal cracks, uneven coating surfaces, and non-uniform thicknesses. The interfacial bonding strength of the 1# coatings is notably weak, while the 2# coatings, although slightly better, still display relatively low bonding strength despite having a generally uniform thickness.

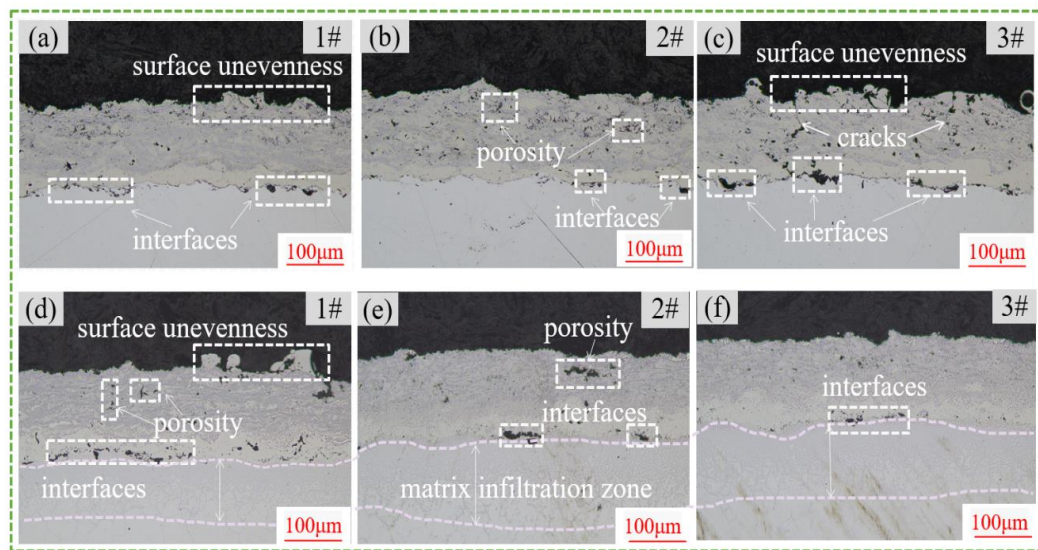


Figure 4. Metallographic structure diagram ((a–c) 1#, 2#, 3# powder coatings before sintering respectively; (d–f) 1#, 2#, 3# powder coatings after sintering respectively).

Figure 5 shows SEM images of the HVOF-sprayed and vacuum-remelted WC-10Co-4Cr/Ni6035WC composite powder coatings. Before sintering, the total coating thickness was approximately 300 µm, including a 100 µm bonding layer of Ni35A. Comparing coatings without vacuum heat treatment reveals a distinct demarcation between the coatings and the substrate, indicating poor bonding. Additionally, there are interconnected pores around the WC in the coatings. The WC agglomeration in the unfired 1# coating, as seen in Figure 6, is more pronounced than in the 2# and 3# coatings due to the higher WC content in the 1# coating. This higher WC content, coupled with lower Ni-based alloy content, leads to inferior coating performance [30–34].

When comparing the porosity of each coating in Figure 6, it is noted that the porosity of the 1# coating increased from 2.86% to 4.89% after vacuum sintering. Additionally, surface roughness increased, and uneven thickness became more evident. However, after vacuum sintering, the porosity issue in the 2# coating significantly improved, reducing to 3.41%. The demarcation at the interface disappeared, and bonding strength was enhanced. In the 3# coating, large pores, cracks, and other defects were notably reduced after vacuum sintering, leaving only small round pores. The porosity was decreased to 1.43%, and issues like uneven thickness and surface roughness were largely resolved. Overall, the coating thickness was maintained at around 280 µm post-sintering without significant shrinkage, and a matrix penetration zone of approximately 150 µm thick was formed between the coating and the substrate due to the mutual diffusion of alloying elements from the powder and the surface of the 316 stainless-steel substrate. Defects such as holes and cracks in the 2# and 3# coatings were significantly improved, and the WC particles were more effectively wetted, transforming connected pores into closed pores. This improvement is attributed to the low melting point of elements like B and Si in the powder. During the sintering process, these elements melted and reformed the deformed particles into a liquid alloy, eliminating gases and impurities from the sprayed layer.

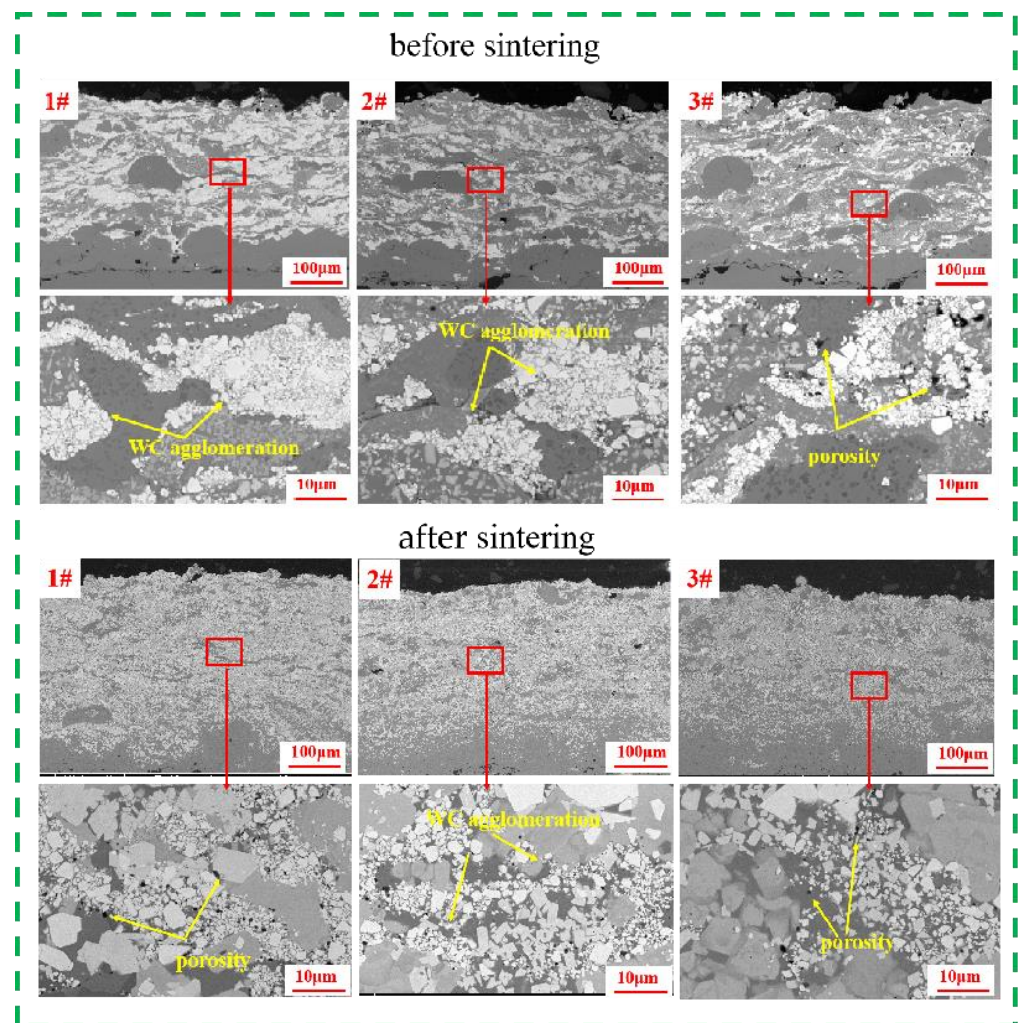


Figure 5. SEM images of HVOF sprayed and vacuum remelted WC-10Co-4Cr/Ni6035WC composite powder coated cross-section.

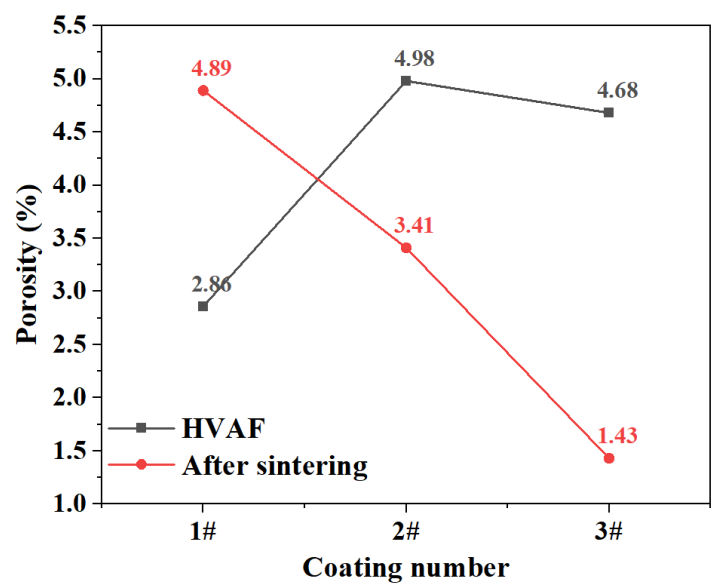


Figure 6. Change in coating porosity before and after sintering.

3.2. Microhardness Observations

As illustrated in Figure 7, the hardness of each coating increased by 5.49% after vacuum remelting compared to their hardness before sintering, indicating that the vacuum sintering process at 1120 °C significantly enhances the coatings' hardness. Specifically, the hardness of the unsintered 1# coating is 966 HV, which is notably higher than the 906 HV and 845 HV measured for the 2# and 3# coatings, respectively. This difference is attributed to the higher WC-10Co-4Cr content in the 1# coating, along with its lower porosity and the absence of cracks. The improvement in hardness is further supported by the precipitation of chromium carbide and borides during sintering, which, coupled with the uniform heating provided by vacuum sintering, leads to a uniform microstructure, the elimination of cracks, and enhanced densification [35].

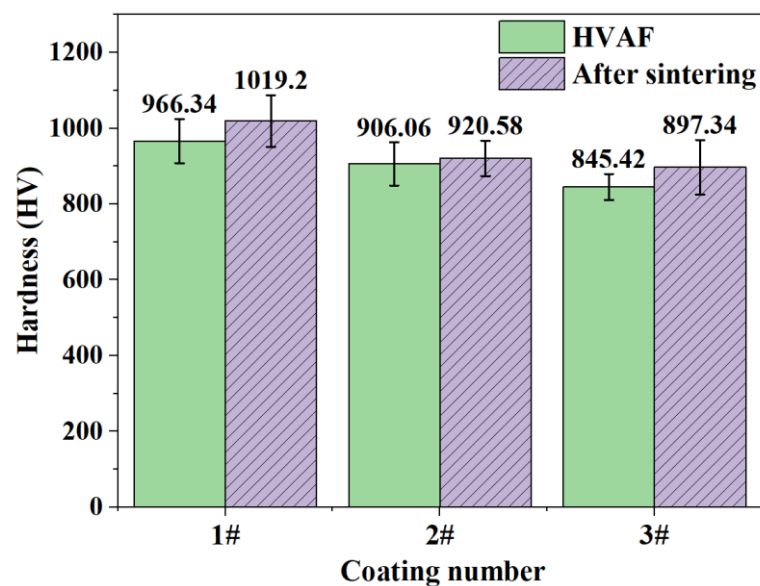


Figure 7. Variation in hardness of each coating before and after sintering.

Despite the increase in porosity after sintering, the 1# coating's hardness remains the highest among all the coatings due to its elevated WC content [36,37]. Additionally, it was observed that the average microhardness of the substrate penetration zone formed after sintering reached 354 HV, representing a 77% increase compared to the substrate's original hardness of 208 HV.

3.3. Friction Wear Performance Analysis

Figure 8 presents the 2D wear images of coatings with varying WC-10Co-4Cr contents before and after sintering. It is evident from these images that the 1# coating exhibits the deepest wear marks and the highest wear volume, both before and after sintering, whereas the 3# coating shows the shallowest wear marks and the least wear. Figure 9 further illustrates the changes in average wear rates for these coatings before and after vacuum sintering. Post-vacuum remelting, the average wear rate of the 1# coating decreases by 6%, while the wear rates for the 2# and 3# coatings decrease by 13%, indicating that vacuum sintering significantly enhances the abrasion resistance of the coatings. Notably, coating 3# consistently demonstrates the lowest average wear rate, both before and after sintering. This suggests that an increase in WC-10Co-4Cr content correlates with a higher wear rate and reduced wear resistance, implying that an excessively high WC-10Co-4Cr content does not positively influence the coatings' wear resistance.

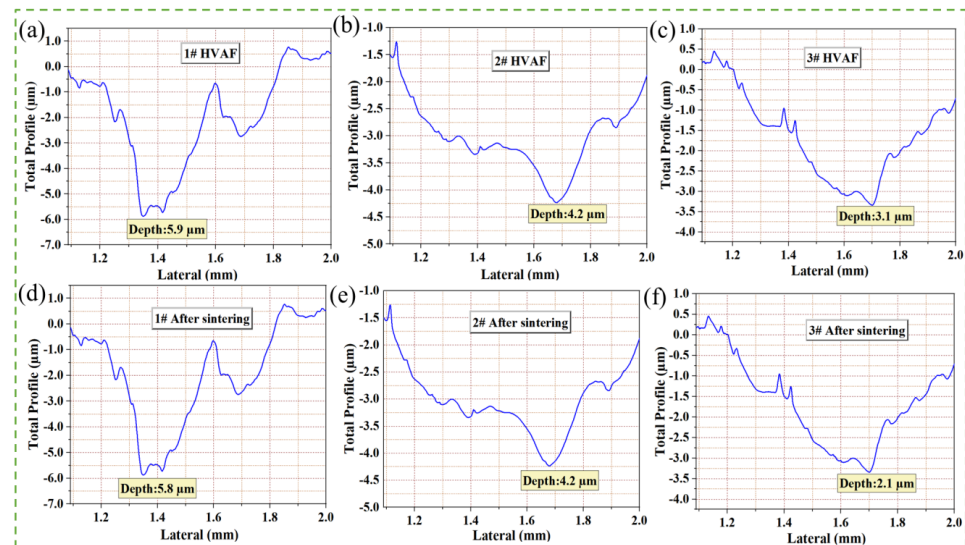


Figure 8. Two-dimensional abrasion marks of coatings with different WC-10Co-4C contents before and after sintering ((a–c), samples before sintering; (d–f) samples after sintering).

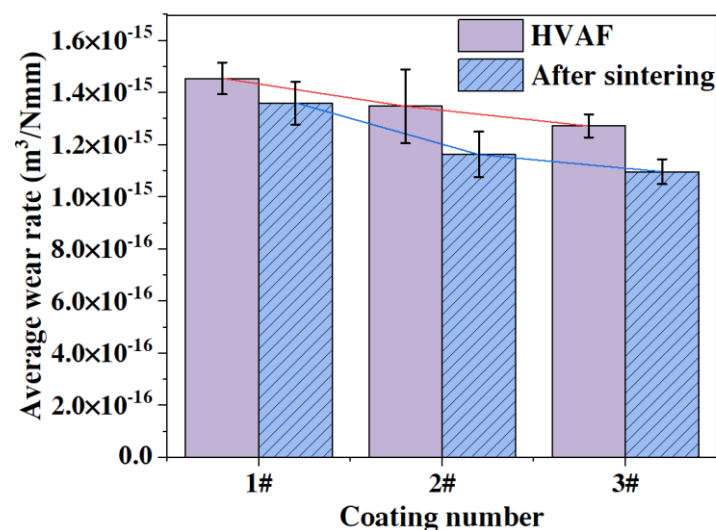


Figure 9. Change in average wear rate of each coating before and after sintering.

The underlying causes of these observations were analyzed based on the wear patterns of the coatings with different WC-10Co-4Cr contents before and after sintering, as depicted in Figure 10. It is apparent that the wear modes of the composite coatings predominantly involve adhesive and oxidative wear, along with fatigue and abrasive wear. Before vacuum remelting, the samples mainly exhibited fatigue and abrasive wear, which is attributed to WC agglomeration and the presence of interconnected pores in the coatings. These factors contribute to poor densification, causing WC particles to be crushed and dislodged during frictional wear, thereby increasing the average wear rate of the coatings [38,39].

The vacuum remelting process led to a more uniform distribution of the coating microstructure, improved densification, increased recrystallization, enhanced bonding strength, and significantly improved the coating's wear resistance. These findings are consistent with the results reported by Rong Hu et al. [18] and are further corroborated by the SEM and friction wear images observed in this study. Comparing Figure 10c with Figure 10a,b reveals more rough pits in the latter two. This phenomenon is likely due to the higher tungsten carbide content in the 1# and 2# coatings and the reduced bonding of nickel to the tungsten carbide particles. Under higher cyclic rolling loads, the tungsten carbide particles in the coatings are dislodged, acting as abrasive particles and

exacerbating the wear [35,40]. The SEM images in Figure 11, showing the wear morphology of coatings with different WC-10Co-4C contents before and after sintering, also support this view. As seen in Figure 11a,b, the excessive WC content leads to a significant aggregation of WC particles within the coating, which hinders the effective encapsulation by metal elements. This results in the fracture and spalling of the WC particles, which can even act as abrasive particles, further exacerbating the wear of the coating. However, this issue is somewhat alleviated after vacuum remelting. The uniformity of the coating improves, and the problem of WC particle aggregation is reduced. By comparing Figure 11c,f, it is evident that after vacuum remelting, the previously aggregated small WC particles are more evenly distributed. Encased in the Ni-based alloy, the bonding strength is enhanced, reducing the likelihood of detachment and better utilizing the wear resistance of WC.

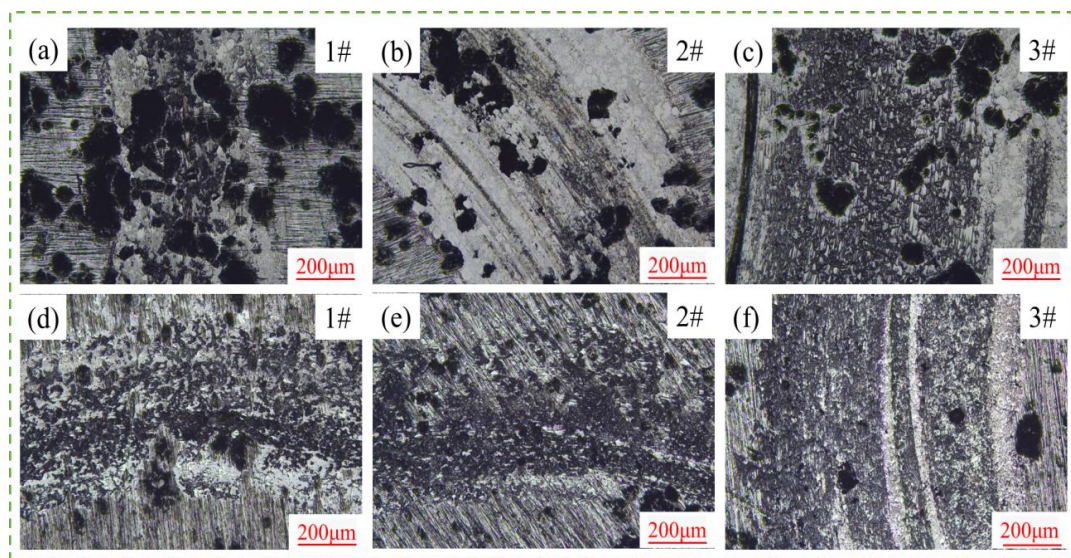


Figure 10. Abrasion morphology of coatings with different WC-10Co-4C contents before and after sintering ((a–c) are unsintered coatings, (d–f) are sintered coatings).

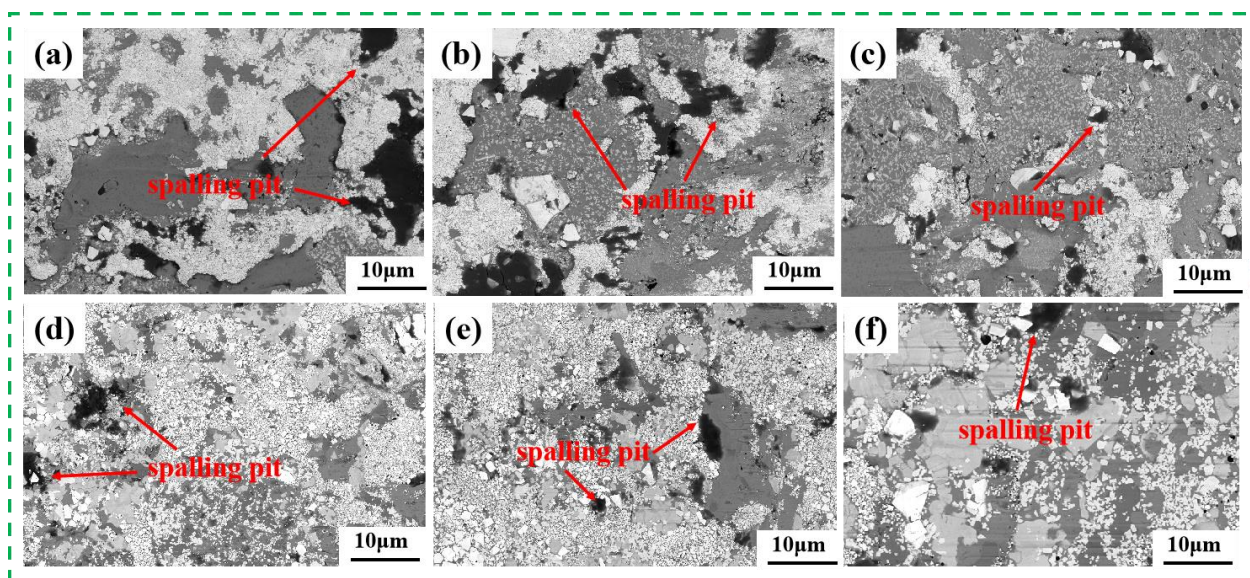


Figure 11. SEM images of wear morphology of coatings with different WC-10Co-4C contents before and after sintering ((a–c) are unsintered coatings, (d–f) are sintered coatings).

The coating wear mechanism was further analyzed through EDS. Figure 12 shows the EDS results of the coating after vacuum remelting, which further confirms that the spalling pits in the coating include cavities formed by the pull-out of fractured WC grains. Additionally, due to the aggregation of WC particles, the encapsulation of elements such as Ni, Co, and Cr around them decreases, leading to the formation of spalling pits. Frequent carbide pull-outs were observed on the worn surface, which is a common material removal mechanism in this type of coating [14,22,41].

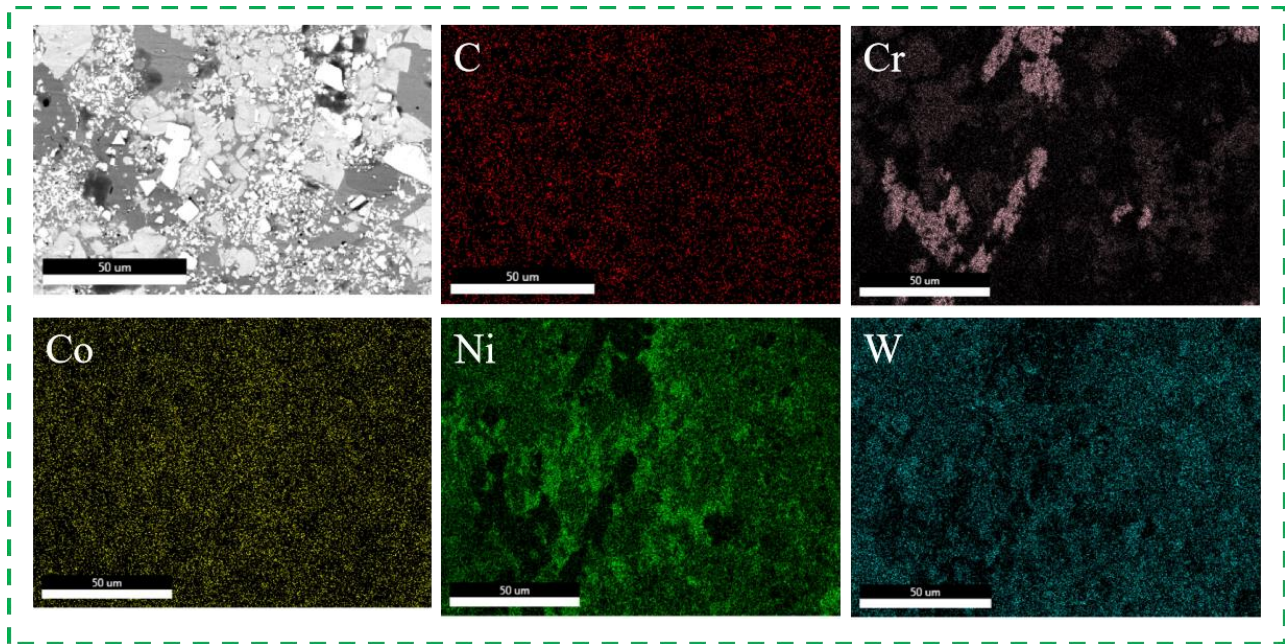


Figure 12. EDS image of abrasion marks of 3# coating after vacuum remelting.

3.4. Scour Resistance Analysis

Figure 13 shows the weight loss during the scouring experiments before and after the sintering of the coatings with different WC-10Co-4Cr contents. Figure 14 shows pictures of the cut surfaces and coating cross-sections after the scouring experiments of the coatings before and after sintering.

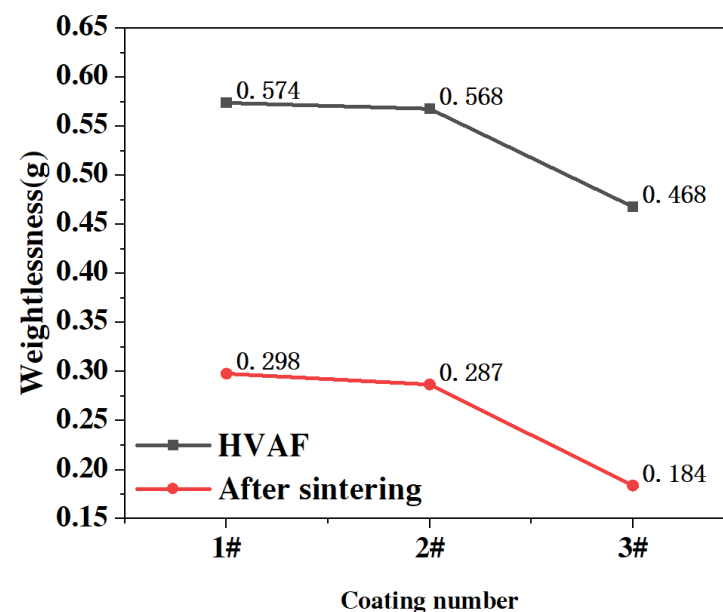


Figure 13. Weight loss of samples before and after sintering in washout experiments.

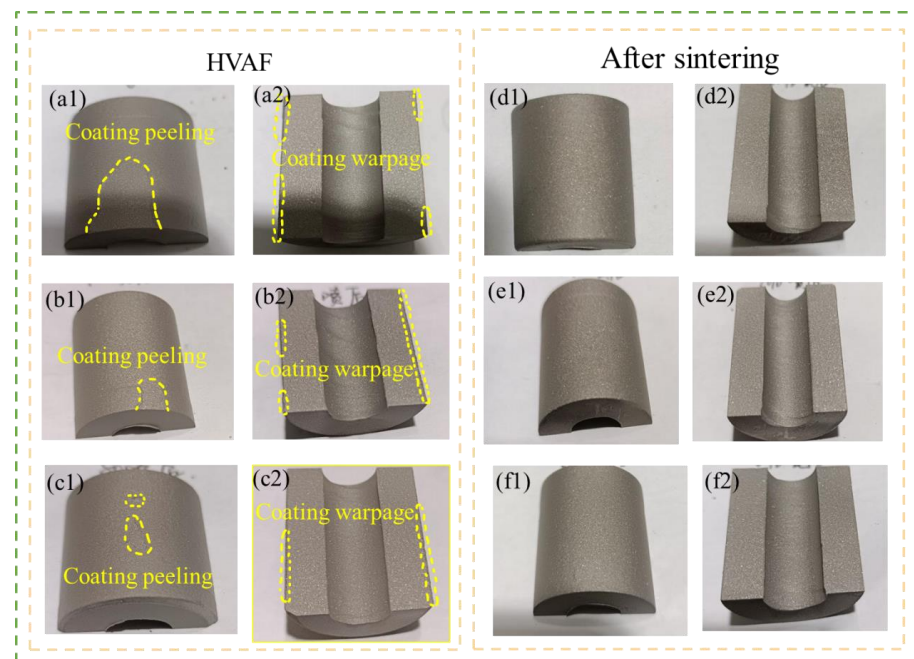


Figure 14. Pictures of cut surfaces and cross-sections of coatings before and after sintering after flushing experiments ((a1,a2) are unsintered 1# samples; (b1,b2) are unsintered 2# samples; (c1,c2) are unsintered 3# samples; (d1,d2) are sintered 1# samples; (e1,e2) are sintered 2# samples; (f1,f2) are sintered 3# samples).

Obviously, vacuum sintering reduced the scour weight loss to a great extent and the scour weight loss of each coating after vacuum sintering was 60% lower than before vacuum sintering, which shows that vacuum sintering can significantly improve the scour resistance of coatings. Meanwhile, the weight loss of the coatings during scouring increases with the increase in WC-10Co-4Cr content in the coatings, whether before or after sintering. The weight loss of the scouring of the 3# coating after sintering is 37% lower than that of the 1# coating and the 3# coating after sintering. The scour resistance of the 3# coating was significantly better than that of the other coatings.

According to Figure 14, it can be found that the coatings before sintering have different degrees of coating peeling and coating warpage on the coating cross-section and cutting surface after the flushing test. The most significant coating peeling and warpage were observed for coating 1#, while coating 3# showed the slightest peeling and warpage. The sintered coatings did not show any coating peeling and warping after the flushing experiment, which is consistent with the weight loss of the coatings before and after the flushing experiment in Figure 13.

It is analyzed that vacuum sintering can effectively improve the scouring resistance of the coatings, which may be the increase in the densification, hardness, and surface flatness of the coatings in the process of sintering; at the same time, the matrix penetration zone generated between the matrix and the coatings can effectively improve the bonding between the coatings and the matrix. The strong scouring resistance of the 3# coatings is due to the low content of WC in the 3# powders, and the fact that the Ni acts as a matrix and a wettable phase, which can bring the WC particles in the coatings to be very well absorbed. Ni, as the matrix and wetting phase, can disperse and encapsulate the WC particles in the coating well and improve the densification of the coating. However, with the gradual increase in WC content, the proportion of Ni-based auto-fusion alloy decreases, resulting in an increase in the density of WC particles. The ability of Ni-based auto-fusion alloy to disperse and wet the encapsulated WC is weakened, and WC agglomeration is obvious, with a lower bonding force of the coating and lower scouring resistance.

4. Conclusions

- (1) Vacuum remelting significantly reduced large pores, cracks, and other coating defects, while achieving metallurgical bonding with the substrate, resulting in a marked increase in hardness within the substrate penetration zone. It also enhanced the coatings' wear resistance, reducing the average wear rate by 6% for coating 1# and 13% for coatings 2# and 3#. These improvements stem from vacuum sintering, which promotes uniform tissue distribution, increased densification, and stronger bonding.
- (2) The 1# coating exhibits higher hardness and wear resistance after HVOF spraying, primarily due to its higher content of WC-10Co-4Cr. However, the increased WC content leads to poorer encapsulation by the nickel-based alloys during vacuum sintering, which in turn reduces the coating's wear resistance compared to other coatings.
- (3) While adding more WC increases the hardness, more is not always better. As WC content increases, the proportion of nickel-based self-fluxing alloy decreases, leading to a higher density of WC particles. This weakens the nickel-based alloy's ability to disperse and wet the WC particles, resulting in noticeable WC agglomeration. Consequently, the coating's bonding strength decreases, and its resistance to erosion is compromised.

The Ni6035WC/Wc-10Cr-4Cr coatings developed in this study effectively enhance the wear and erosion resistance of workpieces, making them highly suitable for applications in waste incineration power generation, deep-sea drilling, and similar industries. These coatings not only extend the service life of the workpieces but also improve operational efficiency, which is of significant importance for conserving and efficiently utilizing resources.

Author Contributions: Conceptualization, X.L. and T.Z.; methodology, X.L. and T.Z.; software, L.L.; validation, X.L., T.Z., and J.H.; formal analysis, S.L.; investigation, Y.L.; resources, X.L.; data curation, T.Z.; writing—original draft preparation, T.Z.; writing—review and editing, L.L.; visualization, B.X.; supervision, Y.W.; project administration, X.S. and Q.H.; funding acquisition, X.L. All authors have read and agreed to the published version of the manuscript.

Funding: This research received no external funding.

Institutional Review Board Statement: Not applicable.

Informed Consent Statement: Not applicable.

Data Availability Statement: Data sharing is not applicable. No new data were created or analyzed in this study.

Acknowledgments: This research was supported by Guangxi Key R&D Programme Projects (No. AB24010346), National Natural Science Foundation of China (No. 52161033,22462003), Reginal Collaboration R&D Program of Sichuan Province under Grant (No. 2024YFHZ0209), the Guangxi key laboratory of Automobile Components and Vehicle technology (2023GKLACVTZZ02), and the Fund Project of the Key Lab of Guangdong for Modern Surface Engineering Technology (No. 2018KFKT01), the Fund Project of the Key Lab of Guangxi Key Laboratory of Automobile Components and Vehicle Technology under under Grant (No. 2022GKLACVTZZ04 and 2023GKLACVTZZ10). Foshan Taoyuan Institute of Advanced Manufacturing (No. TYKF202203001).

Conflicts of Interest: Author Yunsheng Lei was employed by Guangdong Yueke New Material Technology Co., Ltd. The remaining authors declare that the research was conducted in the absence of any commercial or financial relationships that could be construed as a potential conflict of interest.

References

1. Matikainen, V.; Koivuluoto, H.; Vuoristo, P.; Schubert, J. Houdková, Š. Effect of nozzle geometry on the microstructure and properties of HVOF-sprayed WC10Co4Cr and Cr₃C₂-25NiCr coatings. *J. Therm. Spray Technol.* **2018**, *27*, 680–694. [[CrossRef](#)]
2. Kumar, R.K.; Kamaraj, M.; Seetharamu, S.; Pramod, T.; Sampathkumaran, P. Effect of spray particle velocity on cavitation erosion resistance characteristics of HVOF and HVOF processed 86WC-10Co4Cr hydro turbine coatings. *J. Therm. Spray Technol.* **2016**, *25*, 1217–1230. [[CrossRef](#)]

3. Bolelli, G.; Berger, L.-M.M.; Börner, T.; Koivuluoto, H.; Lusvarghi, L.; Lyphout, C.; Markocsan, N.; Matikainen, V.; Nyl, P.; Sassatelli, P.; et al. Tribology of HVOF- and HVOF-sprayed WC–10Co4Cr hardmetal coatings: A comparative assessment. *Surf. Coat. Technol.* **2015**, *265*, 125–144. [\[CrossRef\]](#)
4. Kai, T.A.O.; Zhang, J.; Hua, C.U.I.; Zhou, X.L.; Zhang, J.S. Fabrication of conventional and nanostructured NiCrC coatings via HVOF technique. *Trans. Nonferrous Met. Soc. China* **2008**, *18*, 262–269.
5. Varis, T.; Suhonen, T.; Laakso, J.; Jokipii, M.; Vuoristo, P. Evaluation of residual stresses and their influence on cavitation erosion resistance of high kinetic HVOF and HVOF-sprayed WC–CoCr coatings. *J. Therm. Spray Technol.* **2020**, *29*, 1365–1381. [\[CrossRef\]](#)
6. Janka, L.; Norpoth, J.; Trache, R.; Thiele, S.; Berger, L.M. HVOF- and HVOF-sprayed Cr₃C₂–NiCr coatings deposited from feedstock powders of spherical morphology: Microstructure formation and high-stress abrasive wear resistance up to 800 °C. *J. Therm. Spray Technol.* **2017**, *26*, 1720–1731. [\[CrossRef\]](#)
7. Bolelli, G.; Berger, L.M.; Börner, T.; Koivuluoto, H.; Matikainen, V.; Lusvarghi, L.; Lyphout, C.; Markocsan, N.; Nylén, P.; Sassatelli, P.; et al. Sliding and abrasive wear behaviour of HVOF- and HVOF-sprayed Cr₃C₂–NiCr hardmetal coatings. *Wear* **2016**, *358–359*, 32–50. [\[CrossRef\]](#)
8. Alroy, R.J.; Kamaraj, M.; Sivakumar, G. HVOF vs oxygenated HVOF spraying: Fundamental understanding to optimize Cr₃C₂–NiCr coatings for elevated temperature erosion resistant applications. *J. Mater. Process. Technol.* **2022**, *309*, 117735. [\[CrossRef\]](#)
9. Liu, S.L.; Zheng, X.P. Microstructure and properties of AC-HVOF sprayed Ni60/WC composite coating. *J. Alloys Compd.* **2009**, *480*, 254–258. [\[CrossRef\]](#)
10. Liu, S.; Sun, D.; Fan, Z.; Yu, H.Y.; Meng, H.M. The influence of HVOF powder feedstock characteristics on the sliding wear behaviour of WC–NiCr coatings. *Surf. Coat. Technol.* **2008**, *202*, 4893–4900. [\[CrossRef\]](#)
11. Mahmud, T.B.; Farrokhzad, M.A.; Khan, T.I. Effect of heat treatment on wear performance of nanostructured WC–Ni/Cr HVOF sprayed coatings. *Tribol. Online* **2017**, *12*, 18–28. [\[CrossRef\]](#)
12. Mazouzi, A.; Djerdjare, B.; Triaa, S.; Rezzoug, A.; Cheniti, B.; Aouadi, S.M. Effect of annealing temperature on the microstructure evolution, mechanical and wear behavior of NiCr–WC–Co HVOF-sprayed coatings. *J. Mater. Res.* **2020**, *35*, 2798–2807. [\[CrossRef\]](#)
13. Asl, S.K.; Sohi, M.H.; Hadavi, S.M.M. The effect of the heat treatment on residual stresses in HVOF sprayed WC–Co coating. *Mater. Sci. Forum* **2004**, *465–466*, 427–432.
14. Zhang, Z.; Lei, S.; Xie, X.; Yan, Z.; Li, W.; Zhao, X. Influence of vacuum heat treatment on wear behavior of HVOF sprayed WC–Cr₃C₂–Ni coatings. *Vacuum* **2023**, *216*, 112431. [\[CrossRef\]](#)
15. Xiao, Y. Organization and properties of vacuum sintered fused ni60 coatings. *Met. Heat Treat.* **2017**, *42*, 5.
16. Zhang, Y.; Shuai, G.; Huang, J.; Liu, J. Wx C reinforced Ni-based composite coating in-situ synthesis by laser cladding. *Heat Treat. Met.* **2016**, *41*, 79–83.
17. Mishra, T.K.; Sahu, P.; Gedam, V.; Jain, A.; Atkare, S. Effect of heat treatment on abrasive wear behaviour of Ni–WC coatings. *Mater. Today Proc.* **2023**, S2214785323046205, in press. [\[CrossRef\]](#)
18. Chen, C.; Du, C.; Pan, Q.; Chen, Q. Effect of Post-Heat Treatment on the Microstructure and Mechanical Properties of Laser-Deposited WxC + Ni-Based Composite Thin Walls. *J. Mater. Eng. Perform.* **2021**, *30*, 423–433. [\[CrossRef\]](#)
19. Giacomantonio, M.; Gulizia, S.; Jahedi, M.; Wong, Y.; Moore, R.; Valimberti, M. Heat treatment of thermally sprayed Ni-based wear and corrosion coatings. *Mater. Forum* **2011**, *35*, 48–55.
20. Matikainen, V.; Koivuluoto, H.; Vuoristo, P. A study of Cr₃C₂-based HVOF- and HVOF-sprayed coatings: Abrasion, dry particle erosion and cavitation erosion resistance. *Wear* **2020**, *446–447*, 203188. [\[CrossRef\]](#)
21. Torkashvand, K.; Encalada, A.I.; De Castilho, B.C.N.M.; Gupta, M.; Chromik, R.; Joshi, S. High-temperature sliding wear performance of HVOF sprayed WC-based coatings with alternative binders. *Wear* **2024**, *538–539*, 205206. [\[CrossRef\]](#)
22. Mishra, T.K.; Sahu, P.; Gedam, V. Effect of heat treatment on friction and abrasive wear behavior of WC–12Co microwave cladding. *Mater. Today: Proc.* **2022**, *56*, 373–378. [\[CrossRef\]](#)
23. Wood, R.J.K. Tribology of thermal sprayed WC–Co coatings. *Int. J. Refract. Metals Hard Mater.* **2010**, *28*, 82–94. [\[CrossRef\]](#)
24. Bhosale, D.G.; Prabhu, T.R.; Rathod, W.S. Sliding and erosion wear behaviour of thermal sprayed WC–Cr₃C₂–Ni coatings. *Surf. Coat. Technol.* **2020**, *400*, 126192. [\[CrossRef\]](#)
25. Myalska-Głowacka, H.; Bolelli, G.; Lusvarghi, L.; Cios, G.; Godzierz, M.; Talaniuk, V. Influence of nano-sized WC addition on the microstructure, residual stress, and tribological properties of WC–Co HVOF-sprayed coatings. *Surf. Coat. Technol.* **2024**, *482*, 130696. [\[CrossRef\]](#)
26. Zhang, D.; Peng, Z.; Liu, Z.; Yu, J.; Yuan, L. Study on wear protection performance of HVOF WC–Cr₃C₂–Ni coatings deposited on crystallizer surface. *Surf. Coat. Technol.* **2024**, *481*, 130640. [\[CrossRef\]](#)
27. Gujba, A.K.; Mahdipoor, M.S.; Medraj, M. Water droplet impingement erosion performance of WC-based coating sprayed by HVOF and HVOF. *Wear* **2021**, *484–485*, 203904. [\[CrossRef\]](#)
28. Yu, R.; Zhu, S.; Ding, H.; Luo, Y.; Bai, Y.; Dong, W. Effect of WC content on the organization and properties of WC/Ni60 coatings. *Therm. Process. Technol.* **2023**, *22*, 19–23.
29. Xu, M.; Zhu, S.; Ding, H. Electrical contact strengthening of induction-clad Ni–40% WC composite coatings on 40Cr substrates. *Surf. Coat. Technol.* **2015**, *279*, 32–38. [\[CrossRef\]](#)
30. Hu, C.; Chen, C.; Sun, J.; Wei, S.; Du, Y.; Pan, K.; Wang, C.; Yu, H.; Jiang, T. Comparison of the microstructure and mechanical properties of WC–Ti (C, N)–Ni gradient cemented carbides prepared by SPS pre-sintering and vacuum pre-sintering. *J. Mater. Res. Technol.* **2023**, *26*, 7213–7223. [\[CrossRef\]](#)

31. Wang, C.; Li, W.; Xu, Y.; Luo, X.; Li, Z.; Li, W.; Song, C.; Wang, M.; Zhang, Z.; Huang, C. Effect of WC-17Co content on microstructure, mechanical properties and wear resistance of WC-17Co/Ni composites produced with cold spraying. *Surf. Coat. Technol.* **2024**, *493*, 131252. [[CrossRef](#)]
32. Luo, K.; Ma, H.; He, J.; Lu, J.; He, J.; Wu, N.; Li, C.; Li, Y.; Luo, F. Wear performance of Ni-WC composites and heat-damage behaviour of WC particle during vacuum-induction melting process. *Wear* **2024**, *546–547*, 205294. [[CrossRef](#)]
33. Xu, X.Y.; Xu, B.S.; Liu, W.J.; Liu, S.C.; Zhou, Z.G. Microstructure and properties of vacuum melting CoCrW coating by brazing foil. *Rare Met. Mater. Eng.* **2003**, *32*, 855–858.
34. Tan, X.; Zhu, H.; Zhang, Z.; Zhu, X.; Ni, W.; Li, T.; Kuang, T.; Dai, H.; Zhang, X. Double layer HVAF-sprayed WC-CoCr coatings for optimal properties. *J. Ceram. Int.* **2022**, *48*, 33992–33998. [[CrossRef](#)]
35. Torkashvand, K.; Joshi, S.; Gupta, M. Advances in thermally sprayed WC-based wear-resistant coatings: Co-free binders, processing routes and tribological behavior. *J. Therm. Spray Technol.* **2022**, *31*, 342–377. [[CrossRef](#)]
36. Huttunen-Saarivirta, E.; Heino, V.; Isotandon, E.; Kilpi, L.; Ronkainen, H. Tribocorrosion behaviour of thermally sprayed cermet coatings in paper machine environment. *J. Tribol. Int.* **2019**, *142*, 106006. [[CrossRef](#)]
37. Mahade, S.; Mulone, A.; Bjorklund, S.; Klement, U.; Joshi, S. Investigating loaddependent wear behavior and degradation mechanisms in Cr₃C₂-NiCr coatings deposited by HVAF and HVOF. *J. Mater. Res. Technol.-JMR&T* **2021**, *15*, 4595–4609. [[CrossRef](#)]
38. Hu, R.; Zhang, J.; Wang, R.; Zhang, C.; Xie, Z.; Zhang, Y.; Li, G.; Lu, X. Effect of heat treatment on microstructure and properties of WC reinforced co-based composite coating on copper. *Mater. Lett.* **2022**, *319*, 132262. [[CrossRef](#)]
39. Sadeghimeresht, E.; Markocsan, N.; Nysten, P.; Bjorklund, S. Corrosion performance of bi-layer Ni/Cr₂C₃-NiCr HVAF thermal spray coating. *J. Appl. Surf. Sci.* **2016**, *369*, 470–481. [[CrossRef](#)]
40. Lyphout, C.; Bolelli, G.; Smazalova, E.; Sato, K.; Yamada, J.; Houdková, Š.; Lusvarghi, L.; Manfredini, T. Influence of hardmetal feedstock powder on the sliding wear and impact resistance of High Velocity Air-Fuel (HVAF)sprayed coatings. *Wear* **2019**, *430–431*, 340–354. [[CrossRef](#)]
41. Tian, Y.; Zhang, H.; Chen, X.; McDonald, A.; Wu, S.; Xiao, T.; Li, H. Effect of cavitation on corrosion behavior of HVOF-sprayed WC-10Co4Cr coating with post-sealing in artificial seawater. *Surf. Coat. Technol.* **2020**, *397*, 126012. [[CrossRef](#)]

Disclaimer/Publisher's Note: The statements, opinions and data contained in all publications are solely those of the individual author(s) and contributor(s) and not of MDPI and/or the editor(s). MDPI and/or the editor(s) disclaim responsibility for any injury to people or property resulting from any ideas, methods, instructions or products referred to in the content.